Nonlinear spatiotemporal evolution of whistler mode chorus waves in Earth's inner magnetosphere

Danny Summers,[1,2] Yoshiharu Omura,[3] Yu Miyashita,[3] and Dong-Hun Lee[2]

Received 17 April 2012; revised 23 July 2012; accepted 24 July 2012; published 7 September 2012.

[1] We analyze the nonlinear evolution of whistler mode chorus waves propagating along a magnetic field line from their equatorial source. We solve wave evolution equations off the equator for the wave magnetic field amplitude and wave frequency, subject to boundary conditions at the equator comprising model "chorus equations" that describe the generation of a seed chorus element. The electron distribution function is assumed to evolve adiabatically along a field line. The wave profiles exhibit nonlinear convective growth followed by saturation. Convective growth is due to nonlinear wave trapping, and the saturation process is partly due to a combination of adiabatic effects and a decreasing resonant current with latitude. Notwithstanding computationally expensive full-scale kinetic simulations, our study appears to be the first to analyze the nonlinear evolution and saturation of whistler mode waves off the equator.

Citation: Summers, D., Y. Omura, Y. Miyashita, and D.-H. Lee (2012), Nonlinear spatiotemporal evolution of whistler mode chorus waves in Earth's inner magnetosphere, *J. Geophys. Res.*, *117*, A09206, doi:10.1029/2012JA017842.

1. Introduction

[2] There have been numerous observations of whistler mode Very Low Frequency (VLF), 3–30 kHz, waves in Earth's magnetosphere [e.g., *Storey*, 1953; *Pope*, 1963; *Burtis and Helliwell*, 1969; *Tsurutani and Smith*, 1974; *Anderson and Kurth*, 1989; *Sazhin and Hayakawa*, 1992; *Meredith et al.*, 2001; *Santolik et al.*, 2005; *Spasojevic and Inan*, 2010; *Bunch et al.*, 2011]. Electromagnetic whistler mode chorus emissions typically comprise repeated coherent narrowband signals with rising frequency and can occur in two bands, a lower band, $0.1\sim0.5\Omega_e$, and an upper band, $0.5\sim0.7\Omega_e$, where Ω_e is the local electron gyrofrequency. Chorus is observed outside the plasmasphere to L-shells of about $L = 12$. It is well known that chorus generated near the magnetic equator can be excited by cyclotron resonance with anisotropic 10–100 keV electrons injected near midnight from the plasma sheet [*Kennel and Petshek*, 1966].

[3] Electron gyroresonant interaction with chorus waves is a prime mechanism for generating relativistic (∼1 MeV) electrons in Earth's outer zone, $3 < L < 7$ [*Summers et al.*, 1998, 2002, 2007a, 2007b; *Roth et al.*, 1999; *Horne et al.*, 2003; *Varotsou et al.*, 2005; *Katoh et al.*, 2008; *Xiao et al.*, 2010]. Resonant pitch angle scattering by chorus can cause significant electron precipitation loss from the inner magnetosphere [*Lorentzen et al.*, 2001; *Thorne et al.*, 2005; *Summers et al.*, 2007a, 2007b; *Ni et al.*, 2008; *Lam et al.*, 2010]. Whistler mode waves can act to suppress radiation belt electron fluxes below the so-called Kennel-Petschek limit [*Kennel and Petschek*, 1966; *Summers et al.*, 2009, 2011; *Mauk and Fox*, 2010; *Tang and Summers*, 2012].

[4] While the linear cyclotron resonance theory of *Kennel and Petschek* [1966] is sufficient to explain the basic (linear) phase of the chorus wave generation mechanism, nonlinear theories are required to describe the time-changing chorus frequency and such phenomena as phase bunching and phase trapping. Nonlinear cyclotron resonance theory designed to analyze nonlinear characteristics of whistler mode wave growth and chorus interaction with electrons has been developed by *Dysthe* [1971], *Nunn* [1974], *Matsumoto and Omura* [1981], *Omura et al.* [1991], *Trakhtengerts* [1995], *Albert* [2002], *Omura et al.* [2007, 2008, 2009], and *Summers and Omura* [2007]. In the theory developed by *Omura et al.* [2008, 2009], after the linear growth phase seed chorus emissions with rising frequency are generated near the magnetic equator as a result of a nonlinear growth mechanism that depends on the wave amplitude and that is governed by a relativistic second-order resonance condition. Wave trapping of resonant electrons near the equator causes an electromagnetic electron hole in the wave phase space to be created. The resulting formation of a resonant current then causes nonlinear growth of a wave with rising frequency. Sophisticated numerical codes [*Omura and Summers*, 2006; *Katoh and Omura*, 2006, 2007; *Omura et al.*, 2008; *Hikishima et al.*, 2009, 2010] have provided realistic simulations of the generation of whistler mode chorus and the time-changing features of the growing chorus elements. Further, these

[1]Department of Mathematics and Statistics, Memorial University of Newfoundland, St. John's, Newfoundland, Canada.
[2]School of Space Research, Kyung Hee University, Yongin, South Korea.
[3]Research Institute for Sustainable Humanosphere, Kyoto University, Kyoto, Japan.

Corresponding author: D. Summers, Department of Mathematics and Statistics, Memorial University of Newfoundland, St. John's, NL A1C 5 S7, Canada. (dsummers@mun.ca)

0148-0227/12/2012JA017842

numerical simulations have served to verify various facets of the theory developed by *Omura et al.* [2008, 2009]. *Cully et al.* [2011] recently deduced the sweep rates of chorus elements observed by THEMIS satellites and clearly verified the theoretical sweep rates given by *Omura et al.* [2008, 2009], thereby lending support to the mechanism of nonlinear cyclotron resonant trapping.

[5] In this paper we apply the theory of *Omura et al.* [2008, 2009] to analyze the off-equatorial evolution of whistler mode chorus. Specifically, we assume that a chorus element generated at the equator is determined by a pair of nonlinear ordinary differential equations given by *Omura et al.* [2009; equations (40) and (41)], known as "chorus equations". We then solve a set of wave evolution equations for the wave amplitude and frequency off the equator, using the chorus equations as boundary conditions. We are hence able to demonstrate the nonlinear convective growth and saturation of the waves as they propagate along a magnetic field line. Aside from full-scale kinetic simulations, our study appears to be the first to analyze the nonlinear spatiotemporal evolution of whistler mode waves during propagation from their equatorial source to higher latitudes. We present our model evolution equations in section 2. In section 3 we describe our calculation of the trapped electron distribution, and we present the initial conditions and boundary conditions in section 4. Our numerical results are presented in section 5, and finally we summarize our conclusions in section 6.

2. Model Equations

[6] We assume a coherent electromagnetic whistler mode wave propagating parallel to a background dipole magnetic field, where h is the distance measured along a magnetic field line from the equator. Then, following *Omura et al.* [2008, 2009], we may write the model equations for the wave magnetic field $B_w(h,t)$ and wave frequency $\omega(h,t)$, at position h and time t, in the form,

$$\frac{\partial B_w}{\partial t} + V_g \frac{\partial B_w}{\partial h} = -\frac{\mu_0 V_g}{2} J_E, \tag{1}$$

$$\frac{\partial \omega}{\partial t} + V_g \frac{\partial \omega}{\partial h} = 0, \tag{2}$$

where μ_0 is the vacuum permeability and J_E is the component of the resonant current parallel to the wave electric field. The frequency ω and wave number k are assumed to satisfy the cold-plasma dispersion relation for whistler mode waves, namely,

$$\chi^2 = \frac{1}{1+\xi^2}, \tag{3}$$

where χ and ξ are dimensionless parameters defined by

$$\chi^2 = 1 - \frac{\omega^2}{c^2 k^2}, \tag{4}$$

and

$$\xi^2 = \frac{\omega(\Omega_e - \omega)}{\omega_{pe}^2}. \tag{5}$$

Here, Ω_e and ω_{pe} are respectively the electron gyrofrequency and electron plasma frequency given by

$$\Omega_e = \frac{eB(h)}{m_e}, \qquad \omega_{pe}^2 = \frac{N_e e^2}{\epsilon_0 m_e}, \tag{6}$$

where $B(h)$ is the local value of the background magnetic field strength, N_e is the background electron number density (taken herein as constant), $-e$ is the electron charge, m_e is the electron rest mass, ϵ_0 is the vacuum permittivity (with $\epsilon_0\mu_0 = 1/c^2$), and c is the speed of light. The whistler mode wave group speed V_g is given by

$$V_g = \frac{c\xi}{\chi}\left[\xi^2 + \frac{\Omega_e}{2(\Omega_e - \omega)}\right]^{-1}. \tag{7}$$

The resonant current J_E may be expressed as

$$J_E = -J_0 \int_{\zeta_1}^{\zeta_2} [\cos\zeta_1 - \cos\zeta + S(\zeta - \zeta_1)]^{\frac{1}{2}} \sin\zeta d\zeta, \tag{8}$$

where the gyrophase angles ζ_1 and ζ_2 define the boundary of the trapping wave potential [*Omura et al.*, 2008], and S is the "inhomogeneity parameter" given by

$$S = \frac{-1}{s_0 \omega \Omega_w}\left(s_1 \frac{\partial \omega}{\partial t} + c s_2 \frac{\partial \Omega_e}{\partial h}\right), \tag{9}$$

with

$$s_0 = \frac{\chi}{\xi} \cdot \frac{V_{\perp 0}}{c}, \tag{10}$$

$$s_1 = \gamma_R \left(1 - \frac{V_R}{V_g}\right)^2, \tag{11}$$

$$s_2 = \frac{1}{2\xi\chi}\left\{\frac{\gamma_R \omega}{\Omega_e}\left(\frac{V_{\perp 0}}{c}\right)^2 - \left[2 + \chi^2 \frac{(\Omega_e - \gamma_R \omega)}{(\Omega_e - \omega)}\right]\frac{V_R V_P}{c^2}\right\}, \tag{12}$$

where $\Omega_w = eB_w/m_e$, and $V_{\perp 0}$ is the average perpendicular electron velocity, V_P and V_R are respectively the wave phase velocity and resonant parallel electron velocity, given by

$$V_P = c\chi\xi, \tag{13}$$

and

$$V_R = c\chi\xi\left(1 - \frac{\Omega_e}{\gamma_R \omega}\right), \tag{14}$$

where

$$\gamma_R = \left[1 - \left(\frac{V_R^2}{c^2} + \frac{V_{\perp 0}^2}{c^2}\right)\right]^{-\frac{1}{2}} \tag{15}$$

is the Lorentz factor.

[7] It is useful to obtain from equations (14) and (15) an explicit expression for the resonant velocity V_R in terms of the wave frequency ω, namely,

$$\frac{V_R}{c} = \frac{\frac{1}{\chi\xi}\left(\frac{\omega}{\Omega_e}\right)^2 - \left[\frac{1}{\chi^2\xi^2}\left(\frac{\omega}{\Omega_e}\right)^4 + \left\{\frac{1}{\chi^2\xi^2}\left(\frac{\omega}{\Omega_e}\right)^2 + 1\right\}\left\{1 - \left(\frac{\omega}{\Omega_e}\right)^2 - \left(\frac{V_{\perp 0}}{c}\right)^2\right\}\right]^{\frac{1}{2}}}{\left[\frac{1}{\chi^2\xi^2}\left(\frac{\omega}{\Omega_e}\right)^2 + 1\right]}. \tag{16}$$

An expression for γ_R as an explicit function of ω then follows by substituting result (16) into (15).

[8] We assume that the Earth's dipole magnetic field is approximated by

$$B(h) = B_{eq}\left(1 + ah^2\right), \tag{17}$$

where $B_{eq} = B_E/L^3$ is the equatorial magnetic field strength at a given L-shell, and $a = 4.5/(LR_E)^2$ where R_E is the Earth's radius. Then, from (6) we write

$$\Omega_e = \Omega_{e0}\left(1 + ah^2\right), \tag{18}$$

where $\Omega_{e0} = eB_{eq}/m_e$ is the equatorial electron gyrofrequency. Expression (17) is obtained from a Taylor series expansion, for small magnetic latitude, of the dipole magnetic field strength.

[9] The quantity J_0 appearing in (8) is given by

$$J_0 = (2e)^{\frac{3}{2}}(m_e k\gamma_R)^{-\frac{1}{2}} V_{\perp 0}^{\frac{5}{2}} B_w^{\frac{1}{2}} \chi Q G, \tag{19}$$

where Q is a dimensionless factor representing the depth of the electromagnetic electron hole in phase space within which particle trapping takes place ; G is an "average" value of the assumed hot electron distribution f_t trapped by the wave, defined by

$$G = \left[\int f_t(u_\parallel,\ u_\perp,\ h)du_\perp\right]_{u_\parallel = u_R}, \tag{20}$$

with $u_R = \gamma_R V_R$, $u_\parallel = \gamma v_\parallel$, $u_\perp = \gamma v_\perp$, $\gamma = [1 - (v_\parallel^2 + v_\perp^2)/c^2]^{-1/2}$, where $v_\parallel$ and $v_\perp$ are the parallel and perpendicular electron velocities. We determine the electron distribution f_t and G in the following section.

3. Trapped Electron Distribution f_t

[10] We assume that the hot electron distribution function at the equator takes the form,

$$f_{eq}(u_{\parallel eq},\ u_{\perp eq}) = \frac{N_{eq}}{\pi^{\frac{3}{2}} a_{\parallel eq} a_{\perp eq}^2} \exp\left[-\frac{u_{\parallel eq}^2}{a_{\parallel eq}^2} - \frac{u_{\perp eq}^2}{a_{\perp eq}^2}\right], \tag{21}$$

where N_{eq} is the hot electron number density, and $a_{\parallel eq}$, $a_{\perp eq}$ are the parallel and perpendicular thermal speeds. We further assume that distribution (21) evolves fully adiabatically and we determine the corresponding off-equatorial distribution function. Specifically, we will apply Liouville's theorem that the distribution function is preserved along a particle trajectory (field line), and we will assume that both the first adiabatic invariant and the particle energy are conserved. Writing the off-equatorial distribution in the form,

$$f(u_\parallel,\ u_\perp,\ h) = \frac{N}{\pi^{\frac{3}{2}} a_\parallel a_\perp^2} \exp\left[-\frac{u_\parallel^2}{a_\parallel^2} - \frac{u_\perp^2}{a_\perp^2}\right], \tag{22}$$

we can express Liouville's theorem as

$$f(u_\parallel,\ u_\perp,\ h) = f_{eq}\left(u_{\parallel eq}(u_\parallel,\ u_\perp,\ h),\ u_{\perp eq}(u_\parallel,\ u_\perp,\ h)\right). \tag{23}$$

Preservation of the first adiabatic invariant implies

$$\frac{u_{\perp eq}^2}{B_{eq}} = \frac{u_\perp^2}{B}, \tag{24}$$

and energy conservation gives

$$u_{\parallel eq}^2 + u_{\perp eq}^2 = u_\parallel^2 + u_\perp^2. \tag{25}$$

From equations (24) and (25) we may write

$$u_{\perp eq}^2 = \frac{B_{eq}}{B} u_\perp^2, \tag{26}$$

and

$$u_{\parallel eq}^2 = u_\parallel^2 + \left(1 - \frac{B_{eq}}{B}\right) u_\perp^2. \tag{27}$$

Then, using equations (21), (23), (26), and (27) we find

$$f(u_\parallel,\ u_\perp,\ h) = \frac{N_{eq}}{\pi^{\frac{3}{2}} a_{\parallel eq} a_{\perp eq}^2} \exp\left[-\frac{u_\parallel^2}{a_{\parallel eq}^2} - \left\{\left(1 - \frac{B_{eq}}{B}\right)\frac{1}{a_{\parallel eq}^2} + \frac{B_{eq}}{B}\frac{1}{a_{\perp eq}^2}\right\} u_\perp^2\right]. \tag{28}$$

By comparing (22) and (28) it follows that

$$\frac{N}{a_\parallel a_\perp^2} = \frac{N_{eq}}{a_{\parallel eq} a_{\perp eq}^2}, \tag{29}$$

$$a_\parallel^2 = a_{\parallel eq}^2, \tag{30}$$

and

$$\frac{1}{a_\perp^2} = \left(1 - \frac{B_{eq}}{B}\right)\frac{1}{a_{\parallel eq}^2} + \frac{B_{eq}}{B} \cdot \frac{1}{a_{\perp eq}^2}. \tag{31}$$

Introducing the equatorial thermal anisotropy,

$$A_{eq} = \frac{a_{\perp eq}^2}{a_{\parallel eq}^2} - 1, \tag{32}$$

and making use of the dipole magnetic field approximation (17), we find that equation (31) can be expressed as

$$a_\perp^2 = [W(h)]^2 a_{\perp eq}^2, \tag{33}$$

Table 1. Input Parameters

Parameter		Value
time step	Δt	$10/\Omega_{e0}$
grid spacing	Δh	$5c/\Omega_{e0}$
electron cyclotron frequency at equator	Ω_{e0}	45800 rad/s
electron plasma frequency at equator	ω_{pe}	5 Ω_{e0},10 Ω_{e0}
plasma frequency of hot electrons	ω_{eq}	0.1 Ω_{e0}
depth of electron hole	Q	0.5
average perpendicular velocity	$V_{\perp 0}$	0.3 c
perpendicular thermal speed	$a_{\perp eq}$	0.355 c
parallel thermal speed	$a_{\parallel eq}$	0.212 c
L-shell	L	4.54
coefficient of parabolic magnetic field	a	$1.5 \times 10^{-7}\ \Omega_{e0}^2/c^2$

where

$$W(h) = \left(1 + \frac{A_{eq} a h^2}{1 + a h^2}\right)^{-\frac{1}{2}}. \tag{34}$$

The off-equatorial electron distribution f is hence given by (22), subject to conditions (29), (30), and (33).

[11] Finally, to obtain the desired form of the trapped electron distribution f_t we set

$$f_t(u_\parallel,\ u_\perp,\ h) = K \exp\left(-\frac{u_\parallel^2}{a_\parallel^2}\right) \cdot \delta(u_\perp - u_{\perp 0}), \tag{35}$$

where δ is the Dirac delta function , and K, $u_{\perp 0}$ are parameters to be determined by the conditions,

$$\int f_t(u_\parallel,\ u_\perp,\ h) d^3u = \int f(u_\parallel,\ u_\perp,\ h) d^3u, \tag{36}$$

and

$$\int u_\perp f_t(u_\parallel,\ u_\perp,\ h) d^3u = \int u_\perp f(u_\parallel,\ u_\perp,\ h) d^3u, \tag{37}$$

where $d^3u = 2\pi u_\perp du_\parallel du_\perp$.

[12] From equations (36) and (37) we find

$$2\pi^{\frac{3}{2}} K a_\parallel u_{\perp 0} = N, \tag{38}$$

and

$$4\pi K a_\parallel u_{\perp 0}^2 = N a_\perp, \tag{39}$$

from which it follows that

$$K = \frac{N}{\pi^2 a_\parallel a_\perp}, \quad u_{\perp 0} = \frac{\sqrt{\pi}}{2} a_\perp. \tag{40}$$

Substituting expressions (40) into (35), and making use of (29), (30), and (33), we obtain the trapped electron distribution as

$$f_t(u_\parallel,\ u_\perp,\ h) = \frac{N_{eq} W(h)}{\pi^2 a_{\parallel eq} a_{\perp eq}} \exp\left(-\frac{u_\parallel^2}{a_{\parallel eq}^2}\right) \delta(u_\perp - u_{\perp 0}), \tag{41}$$

where

$$u_{\perp 0} = \frac{\sqrt{\pi}}{2} W(h) a_{\perp eq}. \tag{42}$$

From (20) and (42) we hence find that

$$G = \frac{N_{eq} W(h)}{\pi^2 a_{\parallel eq} a_{\perp eq}} \exp\left(-\frac{u_R^2}{a_{\parallel eq}^2}\right). \tag{43}$$

4. Initial Conditions and Boundary Conditions

[13] In their development of a nonlinear growth theory of magnetospheric chorus emissions, *Omura et al.* [2009] have shown that the temporal evolution of whistler mode waves at the magnetic equator can be described by a pair of nonlinear coupled differential equations, referred to as "chorus equations". In the present study we adopt these equations as boundary conditions at the magnetic equator ($h = 0$) in our numerical solution of the spatiotemporal evolution equations (1) and (2). Setting $\tilde{B}_w = B_w(0,\ t)/B_{eq}$, $\tilde{\omega} = \omega(0, t)/\Omega_{e0}$, and $\tilde{t} = \Omega_{e0} t$, we write these chorus equations as

$$\frac{\partial \tilde{B}_w}{\partial \tilde{t}} = \frac{\Gamma_N}{\Omega_{e0}} \tilde{B}_w - \frac{5 s_2}{s_0} \left(\frac{V_g}{c}\right) \frac{\tilde{a}}{\tilde{\omega}}, \tag{44}$$

$$\frac{\partial \tilde{\omega}}{\partial \tilde{t}} = \frac{2 s_0}{5 s_1} \tilde{\omega} \tilde{B}_w, \tag{45}$$

where V_g, s_0, s_1 and s_2, which are all defined above in section 2, are evaluated at the equator ($h = 0$) and are expressible as functions of $\tilde{\omega}$; $\tilde{a} = ac^2/\Omega_{e0}^2$; Γ_N is the nonlinear wave growth rate given by

$$\frac{\Gamma_N}{\Omega_{e0}} = \frac{\sqrt{2} Q \chi^{\frac{3}{2}}}{\tilde{B}_w^{\frac{1}{2}} \tilde{\omega}^{\frac{1}{2}}} \left(\frac{\xi}{\gamma_R}\right)^{\frac{1}{2}} \left(\frac{V_g}{c}\right) \left(\frac{V_{\perp 0}}{c}\right)^{\frac{5}{2}} \left(\frac{\omega_{pe}}{\Omega_{e0}}\right)^2 \cdot \frac{c^2 G}{N_e}, \tag{46}$$

where G and all other parameters on the right-hand side are evaluated at $h = 0$. Equations (44) and (45) are valid for wave amplitudes satisfying $\tilde{B}_w > \tilde{B}_{th}$ where $\tilde{B}_{th}$ is the threshold value,

$$\tilde{B}_{th} = \frac{25}{2} \frac{\xi \gamma_R}{\chi^5 \tilde{\omega}} \left(\frac{\tilde{a} s_2}{Q}\right)^2 \left(\frac{c}{V_{\perp 0}}\right)^7 \left(\frac{\Omega_{e0}}{\omega_{pe}}\right)^4 \frac{N_e^2}{(c^2 G)^2}, \tag{47}$$

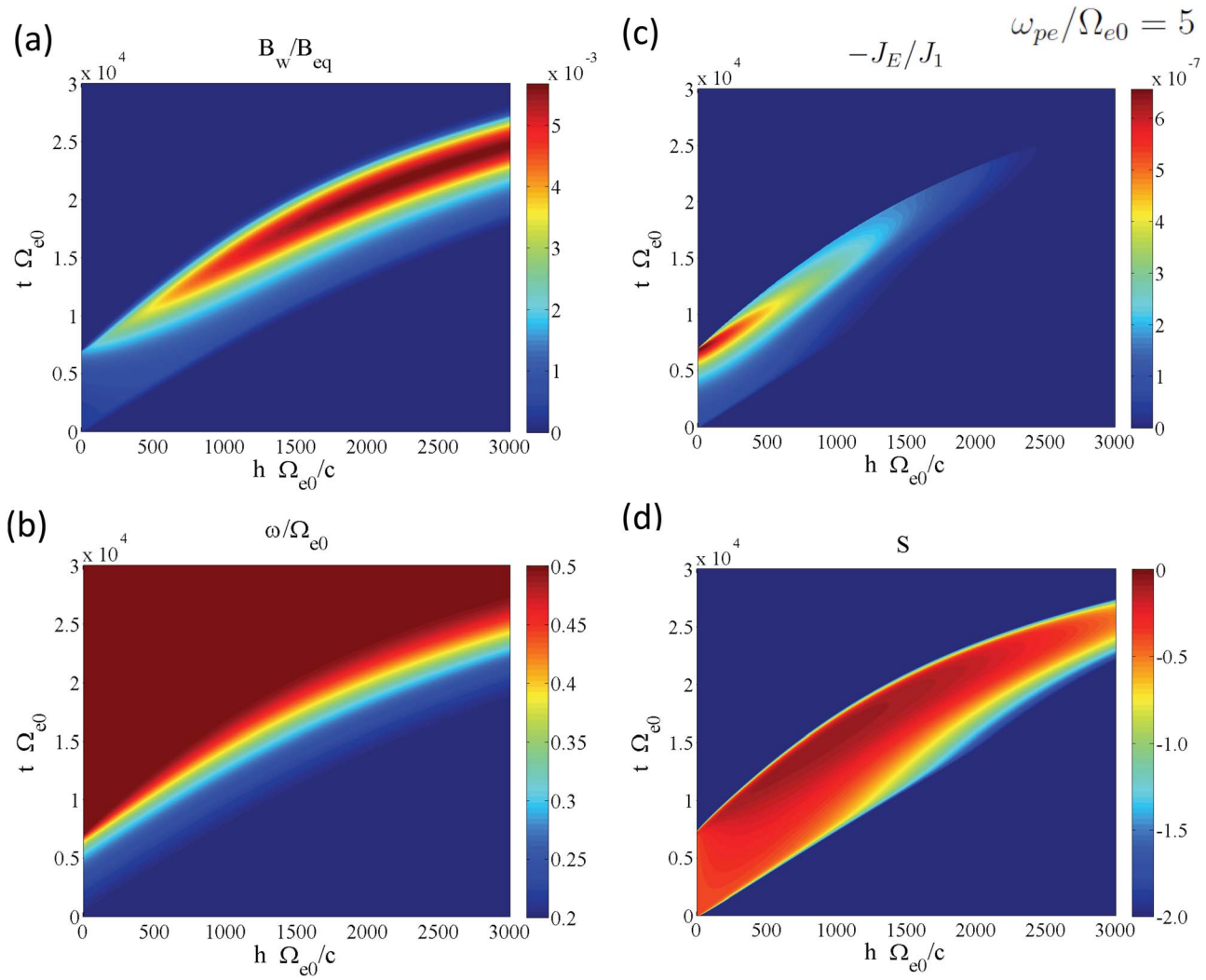

Figure 1. Two-dimensional plots, with respect to latitudinal spatial variable $h\Omega_{e0}/c$ and time variable $t\Omega_{e0}$, of (a) dimensionless wave amplitude B_w/B_{eq}, (b) dimensionless wave frequency ω/Ω_{e0}, (c) dimensionless resonant current $-J_E/J_1$, and (d) inhomogeneity parameter S. For these plots, we set $\omega_{pe}/\Omega_{e0} = 5$, and $\tilde{B}_{w0} = B_w(0,0)/B_{eq} = 3.5 \times 10^{-4}$. Normalized threshold wave amplitude, calculated from (48), is $\tilde{B}_{th} = 3 \times 10^{-4}$.

evaluated at $h = 0$. As initial conditions for equations (44) and (45), we choose $\tilde{B}_w(0,0) = \tilde{B}_{w0}$, $\tilde{\omega}(0,0) = \tilde{\omega}_0$ where $\tilde{B}_{w0} \geq \tilde{B}_{th}$, and $\tilde{\omega}_0 = 0.2$. We solve equations (44) and (45) over the time interval $0 \leq \tilde{t} \leq \tilde{t}_1$ where $\tilde{t}_1$ corresponds to the time at which $\tilde{\omega} = \tilde{\omega}_1$, where we set $\tilde{\omega}_1 = 0.5$. For times satisfying $\tilde{t} > \tilde{t}_1$, we put $\tilde{B}_w(0,\tilde{t}) = 0$ and $\tilde{\omega}(0,\tilde{t}) = \tilde{\omega}_1$. Initially, for $h > 0$, we put $\tilde{B}_w(h,0) = 10^{-2}\tilde{B}_{w0}$ and $\tilde{\omega}(h,0) = \tilde{\omega}_0$. The cut-off in the wave frequency at $\tilde{\omega}_1 = 0.5$ is introduced artificially. Since our model assumes parallel wave propagation, it is not possible to simulate the formation of the gap at half the electron gyrofrequency naturally.

5. Numerical Results

[14] We now report our results based on numerical solutions of the model equations (1) and (2) for the wave magnetic field $B_w(h, t)$ and wave frequency $\omega(h, t)$. Values of the chosen input parameters, including the time step and grid spacing used in our calculations, are given in Table 1. In particular we choose the L-shell value $L = 4.54$. In Figure 1, in which we set $\omega_{pe}/\Omega_{e0} = 5$, we show two-dimensional plots of (a) normalized wave amplitude, (b) normalized wave frequency, (c) normalized resonant current $-J_E/J_1$, where $J_1 = 2eB_{eq}^2/(\mu_0 m_e V_g)$, and (d) the inhomogeneity parameter S given by (9). In Figure 2, corresponding to each of the variables plotted in Figure 1, we show line plots against time at the specified latitudinal locations. As we stated in section 4, we solve the evolution equations (1) and (2) for B_w and ω subject to the condition that a chorus element, as given by (44)–(45), is generated at the equator, $h = 0$. To simulate lower-band chorus, this initial chorus element is specified over the frequency range $0.2 < \tilde{\omega} < 0.5$. Figures 1b and 2b show how the frequency profile is

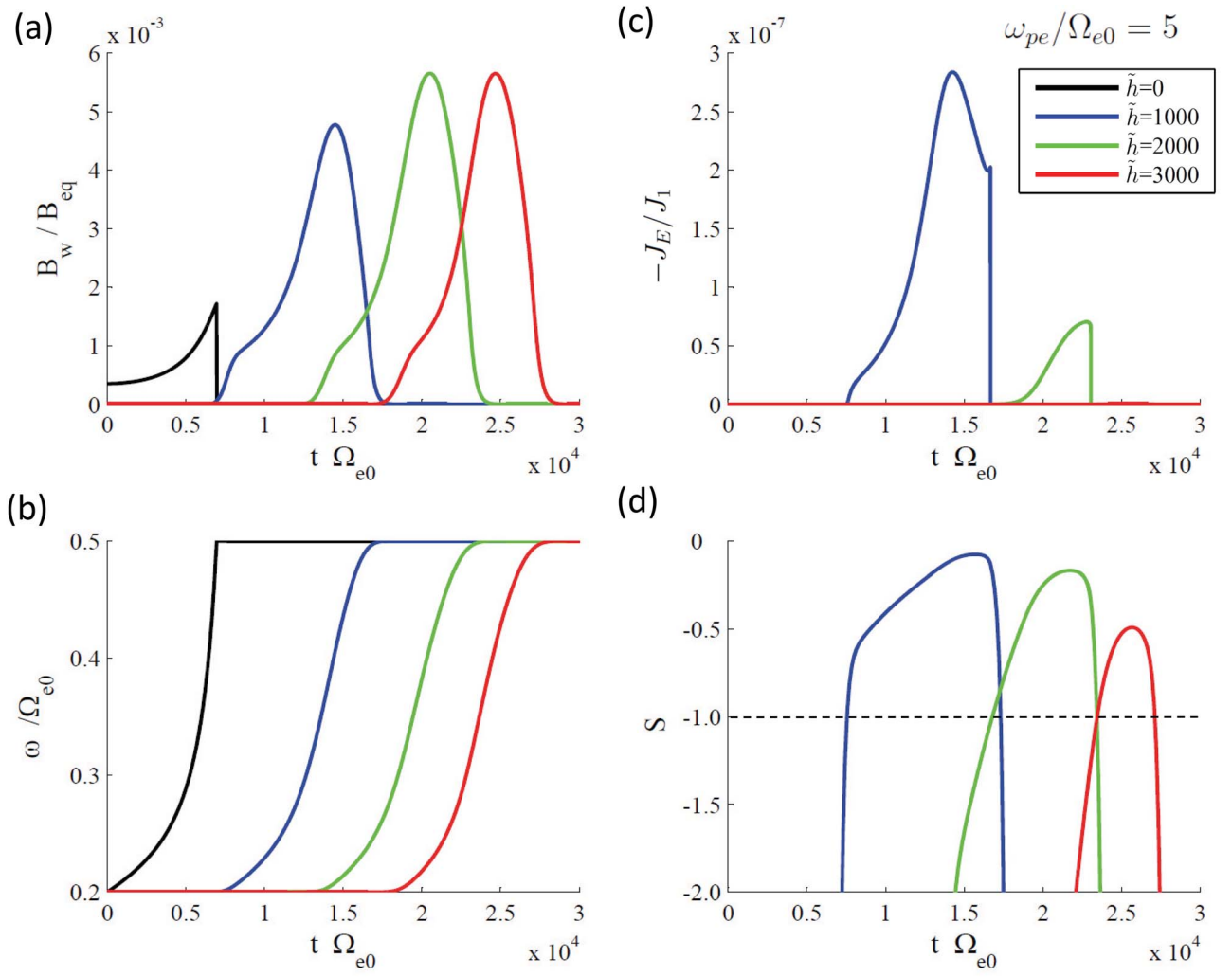

Figure 2. Corresponding to Figure 1, line plots against time $t\Omega_{e0}$ of the wave amplitude B_w/B_{eq}, wave frequency ω/Ω_{e0}, resonant current $-J_E/J_1$, and inhomogeneity parameter S, each at the specified latitudinal distances $\tilde{h} = h\Omega_{e0}/c$.

maintained during propagation off the equator. Figures 1a and 2a show the nonlinear convective growth, i.e., increasing wave amplitude, as the chorus element evolves to higher latitudes. Further, Figures 1a and 2a show wave saturation during propagation to higher latitudes due to adiabatic effects and a rapidly decreasing energetic electron flux. This decreasing electron flux is equivalent to a decreasing resonant current (see Figures 1c and 2c) or a decreasing value of the parameter G. Here, note that $J_0 \propto G$ (from (19)), $G \propto \exp(-u_R^2/a_{\parallel eq}^2)$ (from (43)), $u_R = \gamma_R V_R$, and the magnitude of the resonant parallel electron velocity $|V_R|$ increases as h increases [e.g., see *Omura and Summers*, 2006, Figure 1].

[15] Wave growth and frequency increase take place during the formation of the electromagnetic electron hole in space-time regions where $-1 < S < 0$. These regions can be readily identified in Figures 1d and 2d.

[16] Figures 3 and 4 are similar in format to Figures 1 and 2 except that we set $\omega_{pe}/\Omega_{e0} = 10$. Therefore, since $\omega_{pe} \propto \sqrt{N_e}$, Figures 3 and 4 apply to a denser cold plasma than Figures 1 and 2. The results in Figures 3 and 4 are qualitatively very similar to those in Figures 1 and 2, though there are marked quantitative differences. Figures 3b and 4b show that the chorus element takes longer to propagate to a given latitudinal location than for the lower cold-density case (indicated in Figures 1b and 2b). The threshold wave amplitude is much less in the $\omega_{pe}/\Omega_{e0} = 10$ case than in the $\omega_{pe}/\Omega_{e0} = 5$ case (the respective values being $\tilde{B}_{th} = 4 \times 10^{-6}$ and $\tilde{B}_{th} = 3 \times 10^{-4}$). However, the maximum value of the wave amplitude attained in the denser cold plasma case is only slightly less than for the lower cold-density case (compare Figures 3a and 4a with Figures 1a and 2a). The maximum value attained by the resonant current in the denser cold plasma case is less by more than a factor of 2 (compare Figures 3c and 1c). Comparison of Figures 3d and 4d with Figures 1d and 2d shows that the formation of an electron

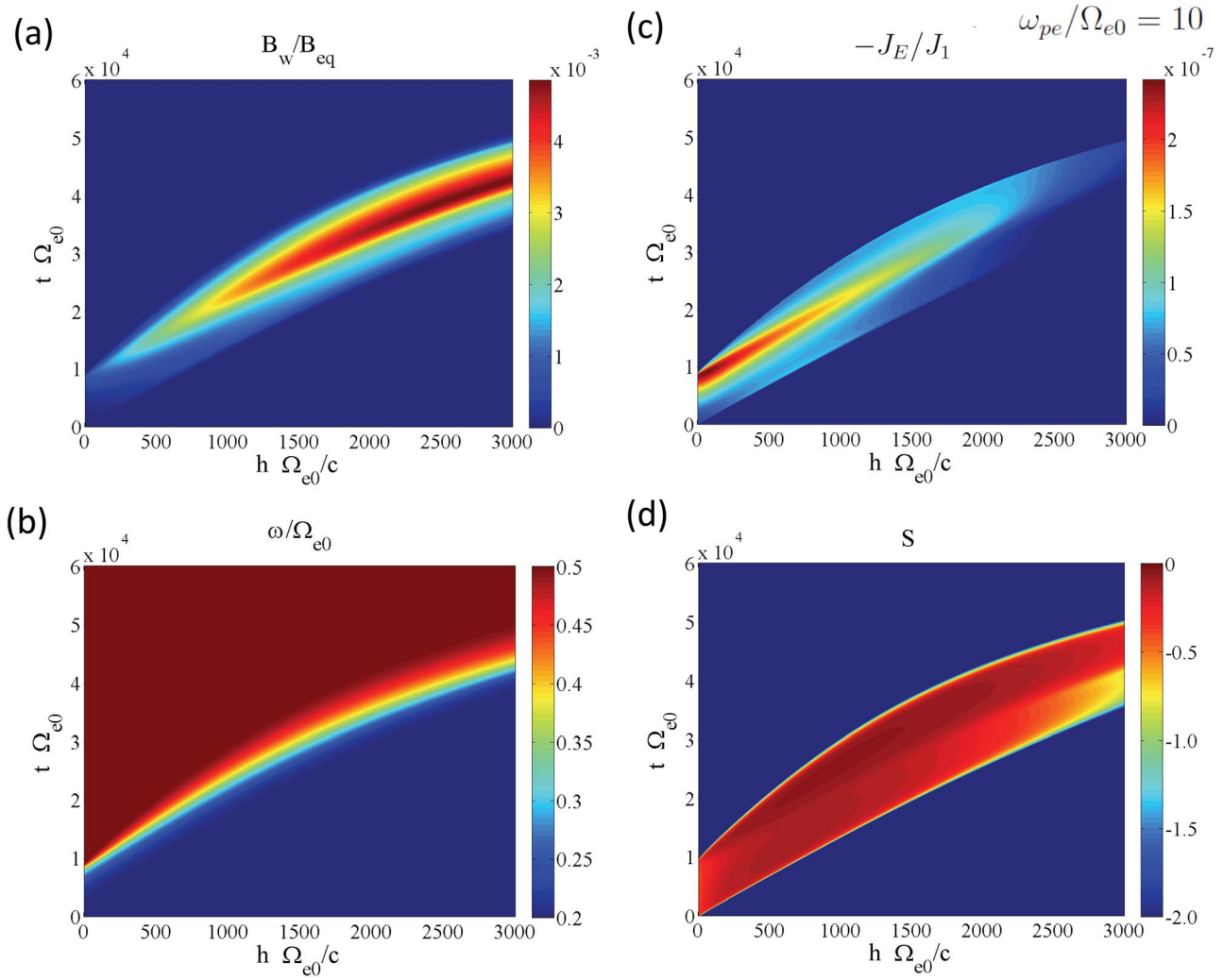

Figure 3. As in Figure 1, except here we set $\omega_{pe}/\Omega_{e0} = 10$, and $\tilde{B}_{w0} = 5 \times 10^{-6}$. Normalized threshold wave amplitude is $\tilde{B}_{th} = 4 \times 10^{-6}$.

hole (with $-1 < S < 0$) at a given latitude takes place at a later time than for the lower cold-density case.

[17] It is also of interest to consider how the latitudinal distance, say h_g, over which sustained wave growth takes place, varies with the cold plasma density. For $\omega_{pe}/\Omega_{e0} = 5$, from Figures 1 and 2 we estimate that $h_g \sim 12{,}000$ km, while for $\omega_{pe}/\Omega_{e0} = 10$, from Figures 3 and 4, we find $h_g \sim 18{,}000$ km. From these cases, and simulations not shown, we find a clear tendency for h_g to decrease as the cold electron density decreases. The reason for this is as follows. A lower cold density makes the absolute value of the resonance velocity $|V_R|$ increase (by equations (5) and (14)). Then, because of the adiabatic variation of the particle flux, the spatial extent of the region of resonant interaction is more limited for higher values of $|V_R|$.

[18] To supplement the simulations shown in Figures 1–4, we consider how the wave threshold amplitude $\tilde{B}_{th} = B_{th}/B_{eq}$ varies with the cold plasma density and also the hot electron density. We re-write expression (47) in the form,

$$\tilde{B}_{th} = \frac{25}{2}\pi^4 \frac{\xi \gamma_R}{\chi^5 \tilde{\omega}} \left(\frac{\tilde{a} s_2}{Q}\right)^2 \left(\frac{c}{V_{\perp 0}}\right)^7 \left(\frac{\Omega_{e0}}{\omega_{eq}}\right)^4 \left(\frac{a_{\parallel eq}}{c}\right)^2 \left(\frac{a_{\perp eq}}{c}\right)^2 \cdot \exp\left(\frac{2u_R^2}{a_{\parallel eq}^2}\right) \tag{48}$$

where $\omega_{eq} = [N_{eq}e^2/(\epsilon_0 m_e)]^{1/2}$ is the plasma frequency of the hot electrons and N_{eq} is the hot electron number density. In Figure 5a we provide a two-dimensional plot showing the variation of the threshold wave amplitude $\tilde{B}_{th}$ against the normalized cold plasma frequency ω_{pe}/Ω_{e0} and the normalized hot electron plasma frequency ω_{eq}/Ω_{e0}, for the fixed value of wave frequency $\tilde{\omega} = 0.2$. Corresponding to Figure 5a, in Figures 5b and 5c we show respectively

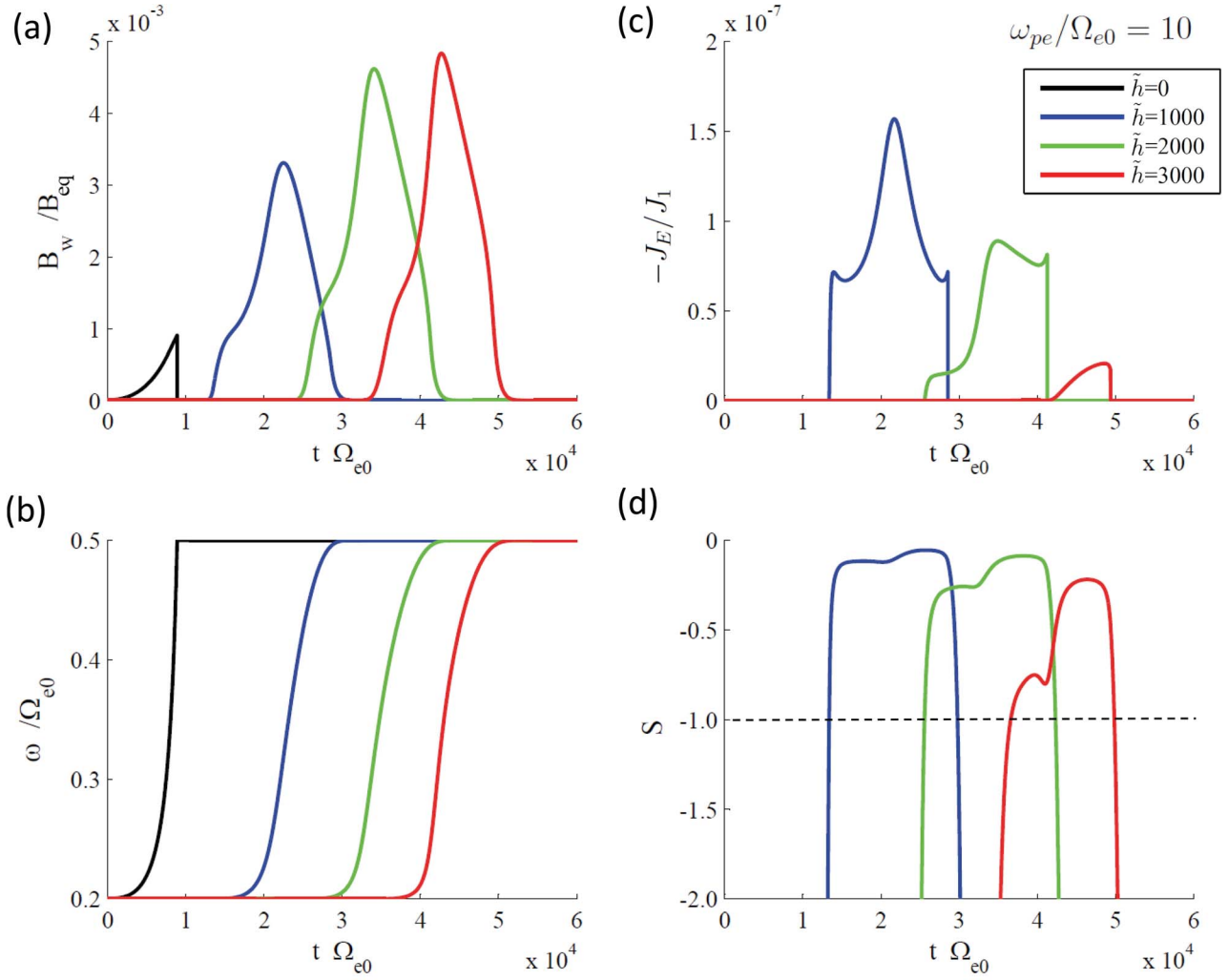

Figure 4. Corresponding to Figure 3, chosen line plots at the specified latitudinal distances $\tilde{h} = h\Omega_{e0}/c$.

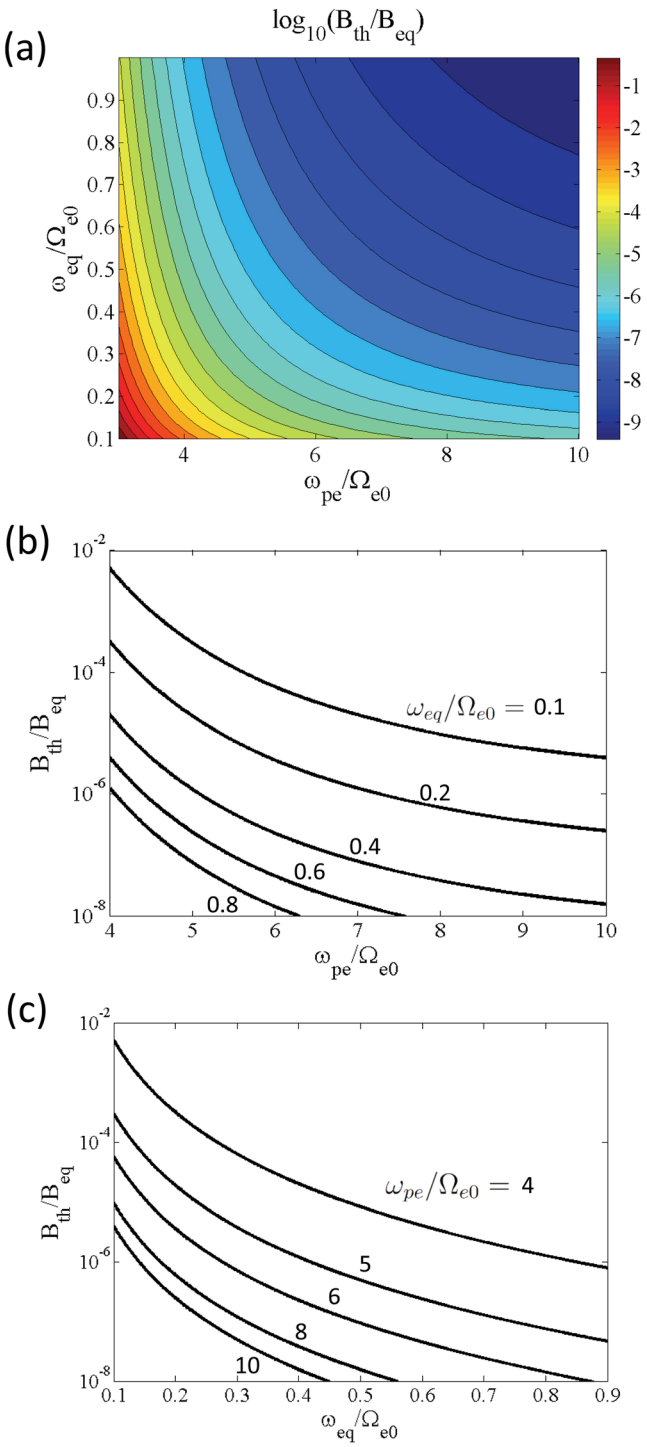

Figure 5. (a) Two-dimensional plot, with respect to the normalized cold plasma frequency ω_{pe}/Ω_{e0} and normalized hot plasma frequency ω_{eq}/Ω_{e0}, of the threshold wave amplitude B_{th}/B_{eq} given by (48), for $\tilde{\omega} = 0.2$. (b) Corresponding to Figure 5a, chosen line plots of B_{th}/B_{eq} against ω_{pe}/Ω_{e0}. (c) Corresponding to Figure 5a, chosen line plots of B_{th}/B_{eq} against ω_{eq}/Ω_{e0}.

chosen line plots of the threshold wave amplitude as functions of the cold and hot plasma frequencies. Clearly, the threshold wave amplitude is a decreasing function of both the cold and hot electron densities (frequencies). This is explained by the fact that a larger cold electron density implies a smaller absolute value of the resonance velocity which in turn implies an increasing flux of resonant electrons.

6. Summary and Conclusions

[19] We assume that whistler mode chorus waves are generated at the magnetic equator, and we examine their nonlinear spatiotemporal evolution along a field line. We solve numerically the wave evolution equations off the equator for the wave magnetic field $B_w(h,t)$ and wave frequency $\omega(h,t)$, subject to boundary conditions at the equator comprising model "chorus equations" that define the generation of a seed chorus element. The electron distribution function is assumed to evolve adiabatically off the equator. We find that the adiabatic variation of the distribution function plays an instrumental role in the saturation process of nonlinear wave growth. Saturation is enhanced by a rapidly decreasing energetic electron flux and decreasing resonant current, at higher latitudes. The present study is the first to monitor the nonlinear growth and saturation of whistler mode chorus waves as they evolve along a field line, aside from computationally expensive full-scale kinetic simulations.

[20] Particle energization by wave trapping and associated wave energy loss are not included in this study, and should be incorporated in a more complete analysis. Evidence from the Cluster spacecraft [*Santolík et al.*, 2009] indicates that in some cases whistler mode chorus waves can propagate obliquely in the source region, so the present theory needs to be extended to include oblique waves. These projects are left for future research.

[21] **Acknowledgments.** This work is supported by a Discovery Grant of the Natural Sciences and Engineering Research Council of Canada to D.S. and by the WCU grant R31-10016 funded by the Korean Ministry of Education, Science, and Technology. Additional support is acknowledged from grant-in-aid 23340147 of the Ministry of Education, Science, Sports and Culture of Japan.

[22] Robert Lysak thanks the reviewers for their assistance in evaluating this paper.

References

Albert, J. M. (2002), Nonlinear interaction of outer zone electrons with VLF waves, *Geophys. Res. Lett.*, *29*(8), 1275, doi:10.1029/2001GL013941.

Anderson, R. R., and W. S. Kurth (1989), Discrete electromagnetic emissions in planetary magnetospheres, in *Plasma Waves and Instabilities at Comets and in Magnetospheres*, *Geophys. Monogr. Ser.*, vol. 53, edited by B. T. Tsurutani and H. Oya, p. 81, AGU, Washington, D. C., doi:10.1029/GM053p0081.

Bunch, N. L., M. Spasojevic, and Y. Y. Shprits (2011), On the latitudinal extent of chorus emissions as observed by the Polar Plasma Wave Instrument, *J. Geophys. Res.*, *116*, A04204, doi:10.1029/2010JA016181.

Burtis, W. J., and R. A. Helliwell (1969), Banded chorus—A new type of VLF radiation observed in the magnetosphere by OGO 1 and OGO 3, *J. Geophys. Res.*, *74*(11), 3002, doi:10.1029/JA074i011p03002.

Cully, C. M., V. Angelopoulos, U. Auster, J. Bonnell, and O. Le Contel (2011), Observational evidence of the generation mechanism for rising-tone chorus, *Geophys. Res. Lett.*, *38*, L01106, doi:10.1029/2010GL045793.

Dysthe, K. B. (1971), Some studies of triggered whistler emissions, *J. Geophys. Res.*, *76*(28), 6915, doi:10.1029/JA076i028p06915.

Hikishima, M., S. Yagitani, Y. Omura, and I. Nagano (2009), Full particle simulation of whistler-mode rising chorus emissions in the magnetosphere, *J. Geophys. Res.*, *114*, A01203, doi:10.1029/2008JA013625.

Hikishima, M., Y. Omura, and D. Summers (2010), Microburst precipitation of energetic electrons associated with chorus wave generation, *Geophys. Res. Lett.*, *37*, L07103, doi:10.1029/2010GL042678.

Horne, R. B., S. A. Glauert, and R. M. Thorne (2003), Resonant diffusion of radiation belt electrons by whistler-mode chorus, *Geophys. Res. Lett.*, *30*(9), 1493, doi:10.1029/2003GL016963.

Katoh, Y., and Y. Omura (2006), A study of generation mechanism of VLF triggered emission by self-consistent particle code, *J. Geophys. Res.*, *111*, A12207, doi:10.1029/2006JA011704.

Katoh, Y., and Y. Omura (2007), Computer simulation of chorus wave generation in the Earth's inner magnetosphere, *Geophys. Res. Lett.*, *34*, L03102, doi:10.1029/2006GL028594.

Katoh, Y., Y. Omura, and D. Summers (2008), Rapid energization of radiation belt electrons by nonlinear wave trapping, *Ann. Geophys.*, *26*, 3451, doi:10.5194/angeo-26-3451-2008.

Kennel, C. F., and H. E. Petschek (1966), Limit on stably trapped particle fluxes, *J. Geophys. Res.*, *71*(1), 1, doi:10.1029/JZ071i001p00001.

Lam, M. M., R. B. Horne, N. P. Meredith, S. A. Glauert, T. Moffat-Griffin, and J. C. Green (2010), Origin of energetic electron precipitation >30 keV into the atmosphere, *J. Geophys. Res.*, *115*, A00F08, doi:10.1029/2009JA014619.

Lorentzen, K. R., J. B. Blake, U. S. Inan, and J. Bortnik (2001), Observations of relativistic electron microbursts in association with VLF chorus, *J. Geophys. Res.*, *106*, 6017, doi:10.1029/2000JA003018.

Matsumoto, H., and Y. Omura (1981), Cluster and channel effect phase bunchings by whistler waves in the nonuniform geomagnetic field, *J. Geophys. Res.*, *86*(A2), 779, doi:10.1029/JA086iA02p00779.

Mauk, B. H., and N. J. Fox (2010), Electron radiation belts of the solar system, *J. Geophys. Res.*, *115*, A12220, doi:10.1029/2010JA015660.

Meredith, N. P., R. B. Horne, and R. R. Anderson (2001), Substorm dependence of chorus amplitudes: Implications for the acceleration of electrons to relativistic energies, *J. Geophys. Res.*, *106*, 13,165, doi:10.1029/2000JA900156.

Ni, B., R. M. Thorne, Y. Y. Shprits, and J. Bortnik (2008), Resonant scattering of plasma sheet electrons by whistler-mode chorus: Contribution to diffuse auroral precipitation, *Geophys. Res. Lett.*, *35*, L11106, doi:10.1029/2008GL034032.

Nunn, D. (1974), A self-consistent theory of triggered VLF emissions, *Planet. Space Sci.*, *22*, 349.

Omura, Y., and D. Summers (2006), Dynamics of high-energy electrons interacting with whistler mode chorus emissions in the magnetosphere, *J. Geophys. Res.*, *111*, A09222, doi:10.1029/2006JA011600.

Omura, Y., D. Nunn, H. Matsumoto, and M. J. Rycroft (1991), A review of observational, theoretical and numerical studies of VLF triggered emissions, *J. Atmos. Terr. Phys.*, *53*, 351.

Omura, Y., N. Furuya, and D. Summers (2007), Relativistic turning acceleration of resonant electrons by coherent whistler mode waves in a dipole magnetic field, *J. Geophys. Res.*, *112*, A06236, doi:10.1029/2006JA012243.

Omura, Y., Y. Katoh, and D. Summers (2008), Theory and simulation of the generation of whistler-mode chorus, *J. Geophys. Res.*, *113*, A04223, doi:10.1029/2007JA012622.

Omura, Y., M. Hikishima, Y. Katoh, D. Summers, and S. Yagitani (2009), Nonlinear mechanisms of lower-band and upper- band VLF chorus emissions in the magnetosphere, *J. Geophys. Res.*, *114*, A07217, doi:10.1029/2009JA014206.

Pope, J. H. (1963), A high-latitude investigation of the natural very-low-frequency electromagnetic radiation known as chorus, *J. Geophys. Res.*, *68*(1), 83, doi:10.1029/JZ068i001p00083.

Roth, I., M. Temerin, and M. K. Hudson (1999), Resonant enhancement of relativistic electron fluxes during geomagnetically active periods, *Ann. Geophys.*, *17*, 631.

Santolik, O., E. Macúšová, K. H. Yearby, N. Cornilleau-Wehrlin, and H. S. K. Alleyne (2005), Radial variation of whistler-mode chorus: First results from the STAFF/DWP instrument on board the Double Star TC-1 spacecraft, *Ann. Geophys.*, *23*, 2937.

Santolík, O., D. A. Gurnett, J. S. Pickett, J. Chum, and N. Cornilleau-Wehrlin (2009), Oblique propagation of whistler mode waves in the chorus source region, *J. Geophys. Res.*, *114*, A00F03, doi:10.1029/2009JA014586.

Sazhin, S. S., and M. Hayakawa (1992), Magnetospheric chorus emissions: A review, *Planet. Space Sci.*, *40*, 681.

Spasojevic, M., and U. S. Inan (2010), Drivers of chorus in the outer dayside magnetosphere, *J. Geophys. Res.*, *115*, A00F09, doi:10.1029/2009JA014452.

Storey, L. R. O. (1953), An investigation of whistling atmospherics, *Philos. Trans. R. Soc. London A*, *246*, 113.

Summers, D., and Y. Omura (2007), Ultra-relativistic acceleration of electrons in planetary magnetospheres, *Geophys. Res. Lett.*, *34*, L24205, doi:10.1029/2007GL032226.

Summers, D., R. M. Thorne, and F. Xiao (1998), Relativistic theory of wave-particle resonant diffusion with application to electron acceleration in the magnetosphere, *J. Geophys. Res.*, *103*(A9), 20,487, doi:10.1029/98JA01740.

Summers, D., C. Ma, N. P. Meredith, R. B. Horne, R. M. Thorne, D. Heynderickx, and R. R. Anderson (2002), Model of the energization of outer-zone electrons by whistler-mode chorus during the October 9, 1990 geomagnetic storm, *Geophys. Res. Lett.*, *29*(24), 2174, doi:10.1029/2002GL016039.

Summers, D., B. Ni, and N. P. Meredith (2007a), Timescales for radiation belt electron acceleration and loss due to resonant wave-particle interactions: 1. Theory, *J. Geophys. Res.*, *112*, A04206, doi:10.1029/2006JA011801.

Summers, D., B. Ni, and N. P. Meredith (2007b), Timescales for radiation belt electron acceleration and loss due to resonant wave-particle interactions: 2. Evaluation for VLF chorus, ELF hiss, and electromagnetic ion cyclotron waves, *J. Geophys. Res.*, *112*, A04207, doi:10.1029/2006JA011993.

Summers, D., R. Tang, and R. M. Thorne (2009), Limit on stably trapped particle fluxes in planetary magnetospheres, *J. Geophys. Res.*, *114*, A10210, doi:10.1029/2009JA014428.

Summers, D., R. Tang, and Y. Omura (2011), Effects of nonlinear wave growth on extreme radiation belt electron fluxes, *J. Geophys. Res.*, *116*, A10226, doi:10.1029/2011JA016602.

Tang, R., and D. Summers (2012), Energetic electron fluxes at Saturn from Cassini observations, *J. Geophys. Res.*, *117*, A06221, doi:10.1029/2011JA017394.

Thorne, R. M., T. P. O'Brien, Y. Y. Shprits, D. Summers, and R. B. Horne (2005), Timescale for MeV electron microburst loss during geomagnetic storms, *J. Geophys. Res.*, *110*, A09202, doi:10.1029/2004JA010882.

Trakhtengerts, V. Y. (1995), Magnetosphere cyclotron maser: Backward wave oscillator generation regime, *J. Geophys. Res.*, *100*(A9), 17,205, doi:10.1029/95JA00843.

Tsurutani, B. T., and E. J. Smith (1974), Postmidnight chorus: A substorm phenomenon, *J. Geophys. Res.*, *79*(1), 118, doi:10.1029/JA079i001p00118.

Varotsou, A., D. Boscher, S. Bourdarie, R. B. Horne, S. A. Glauert, and N. P. Meredith (2005), Simulation of the outer radiation belt electrons near geosynchronous orbit including both radial diffusion and resonant interaction with whistler-mode chorus waves, *Geophys. Res. Lett.*, *32*, L19106, doi:10.1029/2005GL023282.

Xiao, F., Z. Su, H. Zheng, and S. Wang (2010), Three-dimensional simulations of outer radiation belt electron dynamics including cross-diffusion terms, *J. Geophys. Res.*, *115*, A05216, doi:10.1029/2009JA014541.